



Unexpected peak near -15°C in CloudSat echo top climatology

Emily M. Riley¹ and Brian E. Mapes¹

Received 3 February 2009; revised 21 March 2009; accepted 8 April 2009; published 13 May 2009.

[1] We examine a radar-derived climatology of Earth's cloudiness, focusing on the vertical distribution echo tops. Between the two main peaks at ~ 2 km and ~ 14 km associated with low and high clouds, respectively, lie two distinct midlevel peaks in the tropics. One is in the 5–6 km layer, the other between 7 and 8 km. Both are seen day and night, over land and sea, over each tropical ocean basin, and in published ground radar climatology. In the extratropics, the vertical echo top distribution by temperature reveals a strikingly sharp peak in the -15 to -20°C layer (corresponding to the 7–8 km peak in the tropics). Again the signal is robust (night-day, land-sea, summer-winter). We consider interpretations of the -15°C peak ranging from data artifacts (unlikely), to mere radar brightening, to possible true microphysical or dynamical cloudiness enhancement mechanisms. **Citation:** Riley, E. M., and B. E. Mapes (2009), Unexpected peak near -15°C in CloudSat echo top climatology, *Geophys. Res. Lett.*, 36, L09819, doi:10.1029/2009GL037558.

1. Introduction

[2] Among the three cloud étages (high, middle, low), middle clouds are least frequent and arguably the most mysterious. They are often obscured from surface and space optical observation by low and high clouds, respectively, so cloud radar offers the best chance at an unbiased climatology of their occurrence. With CloudSat [Stephens *et al.*, 2002], radar measurements of cloud structure at vertical incidence are now available globally. This study further examines the bimodal distribution of tropical middle clouds identified by Haynes and Stephens [2007], and extends the results to the extratropics using temperature as the vertical coordinate.

[3] Section 2 outlines the data and methods used in this study. Sections 3 and 4 present the tropical and extratropical climatologies of radar echo top occurrence. Section 5 discusses some possible interpretations of the surprising distribution peak near -15°C .

2. Data and Methods

[4] On board CloudSat is a 94 GHz nadir pointing cloud profiling radar (CPR) [Im *et al.*, 2005]. The CPR has a 1.3 km across track by 1.7 km along track nominal footprint, but oversampling results in profiles 1.1 km apart. Vertical bins of 480 m are oversampled to provide a 240 m data resolution. The CPR's minimal detectable signal is about -30 dBZ [Stephens *et al.*, 2008]. We use version 5 the 2B-GEOPROF product, which includes 2D arrays of the radar reflectivity

factor, as well as of a “cloud mask” with a value between 0 and 40. We take values ≥ 20 as indicating hydrometeor echoes (cloud or precipitation).

[5] To simplify and enrich our access to the CloudSat dataset, we devised a hierarchical method of analyzing all hydrometeor (hereafter ‘cloudy’) echoes in the data set, with two tiers: (1) as contiguous echo objects (EOs) and (2) as the pixels comprising EOs.

[6] An EO is defined as a contiguous region (in the radar's vertical sampling plane) of cloud mask ≥ 20 , consisting of at least three pixels with their edges (not merely corners) touching. One and two pixel objects were initially retained, but they were cumbersome (numerous), unimportant to climatology, and often concentrated at low levels near topography suggesting clutter contamination. CloudSat orbit data files begin and end at the equator, so arrays from successive files had to be stitched together at the equator for processing. The first and last three profiles of each orbit have cloud mask values of zero [Marchand *et al.*, 2008], so we re-masked pixels between the surface and 18 km, with reflectivity between -25 dBZ and 30 dBZ, in the first and last 5 columns of each orbit, as cloudy. These choices were based on a study of tropical EOs not affected by the mask problem, and results are not sensitive to these details.

[7] Contiguous EOs in the stitched cloud mask arrays were identified by Interactive Data Language (IDL) routine LABEL_REGION. There are 2,728,616 unique EOs in the one year of data used here. For each EO, we save a top height and geographic information, along with many other attributes.

[8] To assign a temperature profile to each EO, we used European Centre for Medium-range Weather Forecasting (ECMWF) global analysis data, which are available interpolated to the CloudSat grid on a pixel-by-pixel basis in the CloudSat data center's ECMWF-AUX product. Temperature was averaged at each altitude, in the horizontal region spanned by a given EO. In light of the coarser native resolution of the analysis (several 10s of km), this averaging is appropriate for all but the largest EOs (which can span several grid cells in the weather model). Excluding such large EOs does not change our main results or conclusions.

3. Tropical Echo Top Climatology

[9] Figure 1a shows a joint histogram of EO base height versus EO top height for the tropical belt (latitude $< 20^{\circ}$) over ocean and low-altitude land ($z < 1$ km). The EO count histogram is weighted by the horizontal span of each EO, to form a true cloud-cover density. Low-based EOs occur along the vertical axis, while thin layer cloud types lie along the diagonal. A minimum of cloudiness with ~ 3 km EO bases [cf. Zuidema, 1998] separates these distinct deep or precipitating vs. thin layer populations.

[10] EO types are defined by slicing Figure 1a into boxes. The horizontal lines at 4.5 km (approximately the tropical

¹Department of Meteorology and Physical Oceanography, University of Miami, Miami, Florida, USA.

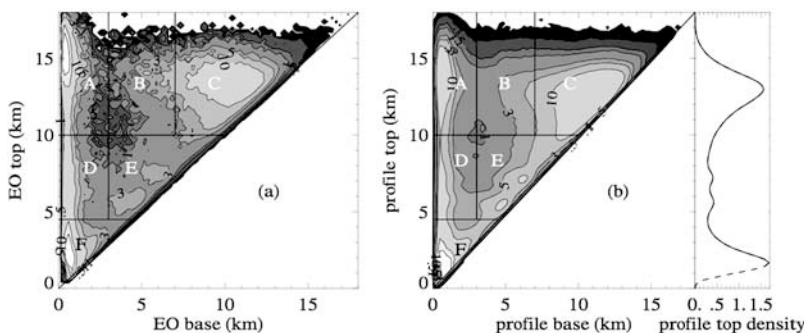


Figure 1. Horizontal cloud cover in the tropics accounted for by clouds with tops and bases in the indicated bins: (a) distribution of cloudiness by EO bases and tops and (b) distribution according to local (echo profile) bases and tops. Contour values (labeled) are in units of 10^3 horizontal echo pixels per bin. Bin size is 240 m by 240 m. Lines and letters delineate EO types, roughly associated to cloud types: A, deep precipitation; B, anvil (thick cirrus); C, cirrus; D, cumulus congestus; E, altostratus and altocumulus; and F, low clouds. The 2D distribution of Figure 1b is integrated at right to show the 1D distribution by local echo top height. Values are in units of %.

0°C level) and 10 km (approximately the height of -40°C) separate warm (liquid water), potentially mixed-phase, and fully glaciated EO tops. These lines also tend to delineate natural types by running through minima in the joint histogram. For middle and high topped EOs, the vertical line (base = 3 km) separates geometrically thick and thin EOs. High-topped EOs are further divided into thicker and thinner by a base = 7 km line. We may roughly associate each box on Figure 1a to a familiar cloud type name as follows: (A) deep precipitation, (B) detached anvil (or thick cirrus) (C) cirrus, (D) cumulus congestus, and (E) altostratus and altocumulus, and (F) low clouds.

[11] Low-topped EOs (type F) represent the most echo cover. High-topped deep EOs (box A) also cover a lot of area, due to their large size when present (an entire echo mass is considered low-based if it precipitates to the surface anywhere.) Thin cirrus are also common, even more so if viewed with greater sensitivity, such as with lidar [Sassen *et al.*, 2008]. This paper's subject is the bimodal population of midlevel (alto) EOs in box E.

[12] A more typical definition of echo top and base distribution – based on individual profiles or columns of radar echo in the atmosphere, rather than EOs – gives similar results (Figure 1b). Panel b, made by processing all the pixels in all tropical EOs, is smoother than panel a, since there are many more profiles than EOs. Nonetheless, the key features are similar in both. Based on this similarity, we will focus on EO top distributions below.

[13] Summing the joint histogram over all base heights in Figure 1b gives the line plot of echo-top density on the right side of Figure 1b. Its units are %, and its interpretation (for the peak value at 2 km) is that about 1.5% of the tropical belt is covered by cloudy echo whose top lies within a 240 m interval of 2 km. The distribution has two dominant peaks at low and high levels, and two smaller mid-level peaks, rendering a curious quad-modal structure.

[14] The 2 km, 5–6 km, and 13 km peaks in tropical cloudiness are commonly explained in terms of convective detrainment at three well known levels of enhanced static stability in the tropics: the trade inversion, the 0°C melting level isotherm, and the tropopause [Johnson *et al.*, 1999]. The mid-level peak around 8 km (near -15°C in the tropics) is not so easily explained. It was first noted in

early CloudSat results from Haynes and Stephens [2007] and can be seen (once it is known to exist) in ARM site cloud radar data [Hollars *et al.*, 2003].

[15] The corresponding distribution of echo cover by EO top (rather than by echo profile top) is shown as a solid curve in Figure 2a. Values are similar to Figure 1b. A breakdown of the EO types contributing to the bimodal mid-level structure is also shown in Figure 2a: The dashed line includes only layer type EOs (in box E of Figure 1a), while the thin solid line indicates the contribution by box D (low-based EOs). The bimodal structure at midlevels is present in both, but is clearest for the layer type EOs, so the remaining panels in Figure 2 focus on those. Figures 2b–2d show that the mid-level bimodal structure in layer type EO top climatology is a robust feature occurring during day and night, over land and ocean, and in each tropical basin (Atlantic, Indian, and West and East Pacific Oceans). A few slight differences can be seen too – land coverage is greater than ocean coverage; the West Pacific has more and higher midlevel cloudiness than the other basins; night (~ 0130 LT) has more than day (~ 1330 LT); the upper peak is relatively enhanced over land. The main point of Figure 2 for present purposes is that the bimodal structure is ubiquitous and robustly sampled.

4. Extratropical CloudSat Climatology

[16] We sought evidence of a similar bimodal structure in the extratropics (20°S/N – 60°S/N). None was apparent in height coordinates, but when EO tops are binned according to temperature, Figure 3 is the result. There is a small yet distinctive peak in the 1D distribution near -15°C (Figure 3), between the dominant low and high cloudiness peaks. Some enhancement near the 0°C level is also seen, but is less cleanly separated from the broad low cloudiness peak than in the tropical profiles. Because the binning is different from Figure 2, absolute values have different units: The upper level maxima in Figure 3 means that about 3% of the extratropical regions are covered by cloudiness whose EO-top temperature is within 2°C of -60°C .

[17] The all-extratropics distribution (thick curve in Figure 3) is further subdivided into day-night, land-ocean, and winter-summer. Day and night overpasses are very similar

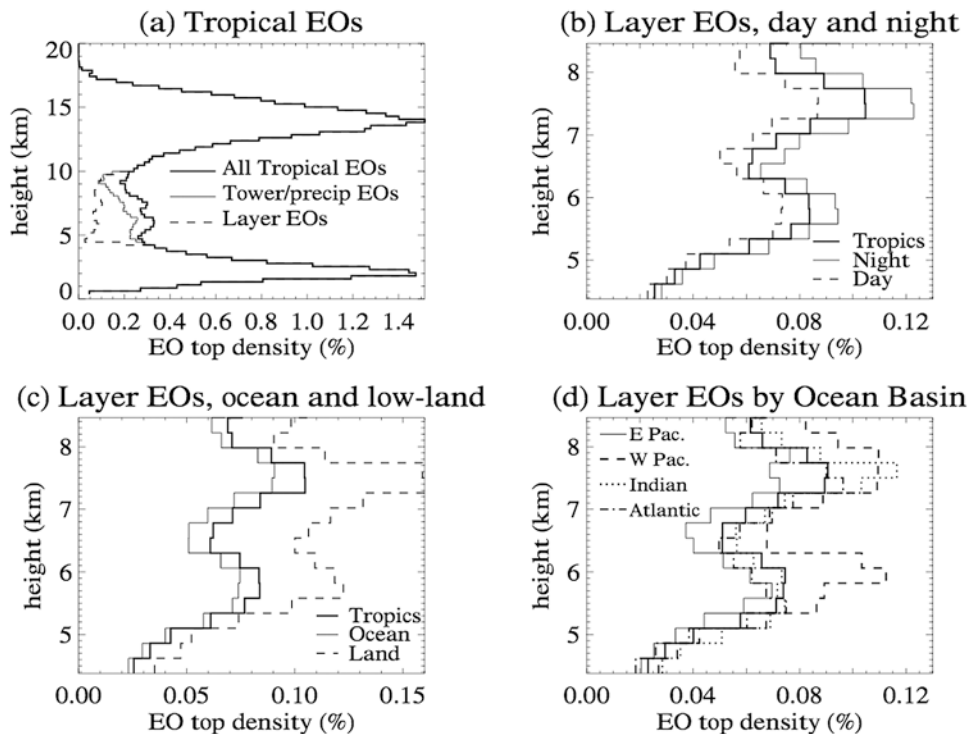


Figure 2. Horizontal cloud cover in the tropics distributed by EO top height. (a) All tropical EOs and midlevel subdivision by layer vs. tower type EOs (types D and E in Figure 1a). (b)–(d) Cloudiness in layer-type EOs (heavy) and indicated subdivisions. The Indian and west and east Pacific are separated at 110°E and 180°W . Bin size is 240 m.

in terms of middle and high EOs (Figure 3a), while low EOs are more common at night. Land is less cloudy than sea, especially at low levels (Figure 3b). The low EO peak in the winter hemisphere is somewhat cooler than in summer (near -5°C rather than $+10^{\circ}\text{C}$, Figure 3c), and the -15°C peak is much clearer in the winter hemisphere, but still distinguishable in summer. The main point, as in Figure 2, is that the peak near -15°C is a robust feature of climatology.

5. Discussion of Possible Interpretations and Mechanisms

[18] The peak in CloudSat observed cloudy-echo top frequency in the -15°C to -20°C range raises several questions: Are we certain it isn't a data processing artifact? If it is a real feature of radar reflectivity climatology, does this indicate an actual enhanced population of clouds, or merely a layer where the particles are more reflective (i.e., a radar 'bright band' as seen at this particular wavelength)? In either case, what might be the physical cause?

[19] A data processing artifact seems extremely unlikely. Haynes and Stephens [2007] found the tropical peak near 8–9 km in an independent study of CloudSat data. No aspect of the cloud mask algorithm [Marchand *et al.*, 2008] could produce a spurious sharp peak, especially not in temperature, as the reflectivity data are handled in geometric height. Furthermore, the peak is discernable in the climatology of cloud radar data from the Manus ARM site [Hollars *et al.*, 2003], with very different sampling and sensitivity constraints.

[20] Is this a true cloud climatology feature, or merely a feature of radar reflectivity detection at the wavelength and

sensitivity limits of CloudSat? One line of evidence suggesting a true cloudiness enhancement near -15°C is the result of Hanna *et al.* [2008], showing a similar sharp peak in infrared (IR) derived cloud tops overlying stations experiencing rain or snow in winter. The study of precipitating locations presumably selects for optically dense clouds, minimizing the smearing effects of optically thin clouds on gross satellite IR temperature distributions. It would be fairly easy to seek such sharp structure in larger samples of IR satellite data, screened in other ways, although finding the tropical peak near 8–9 km would be difficult since it is most common in convectively disturbed conditions (not shown), where visibility is often obscured by higher clouds.

[21] The counter-hypothesis – that the peak is merely from detection enhancement – also has support. Modeling of altocumulus by Sassen and Khvorostyanov [2007] showed that at potentially mixed-phase temperatures (0°C – -40°C), large ice crystals dominate cloud radar reflectivity. The liquid component (numerous but small drops) was found to be difficult to detect at a CloudSat-like sensitivity limit of -28 dBZ. In answer, we can at least confirm that the four modes in Figure 1b persist when the absolute detection threshold is changed, i.e. when echo profile top is redefined as the highest pixel exceeding another threshold like -20 dBZ (not shown). This is weak evidence however, as a microphysical boost in reflectivity at -15°C could simply enhance the frequency of exceedance of all thresholds. Radar reflectivity (Z) goes as mass squared [Hogan *et al.*, 2006, equation 2], in the Rayleigh scattering regime where the small particles near cloud tops presumably reside. How other factors like particle density and crystal habit might affect Z and thus detection frequency is beyond

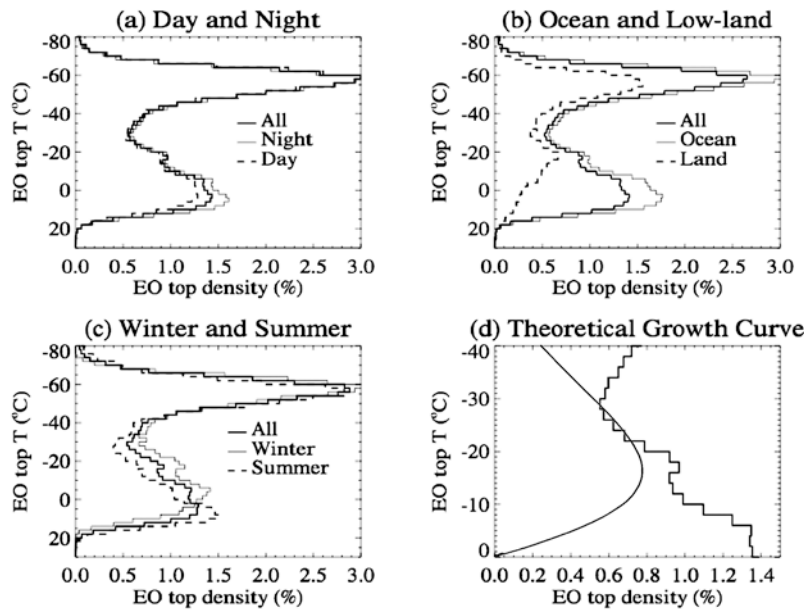


Figure 3. As in Figure 2 but for the extratropics latitudes 20° – 60°N and S. Subdivisions include (a) day and night, (b) ocean and low land (topography <1 km), and (c) winter (JJA (DJF), S. (N) Hemisphere) and summer (DJF (JJA), S. (N.) Hemisphere), and (d) Theoretical growth curve [Rogers and Yau, 1989, Figure 9.4] overlaid with extratropics echo top temperatures between 0° and -40°C . Bin size is 2°C .

our expertise, but these factors [e.g., Hogan *et al.*, 2003] could certainly be temperature dependent.

[22] What is special about temperatures near -15°C ? One possibility is that this is where dendritic ice crystal growth is most rapid. Cloud tunnel laboratory results from Ryan *et al.* [1976] and Fukuta and Takahashi [1999] show a sharp peak in the mass and length growth rates of ice crystals at -15°C . Theoretically derived growth equations show a broad peak near -15°C . Figure 3d shows the growth equation curve [Rogers and Yau, 1989, Figure 9.4] overlaid with the extratropical echo top temperatures between 0°C and -40°C . The broadness of the growth equation curve cannot explain our sharp spike in observation, even though the peak of the curve is at about the right temperature.

[23] Dynamical cloud formation offers another class of hypotheses for the -15°C peak. Enhanced detrainment from deep convection could produce shelf clouds and/or moist layers that could be lifted later to saturation to produce layer clouds. In the tropics at least, the layer-type EO populations with tops near 0°C and -15°C are both associated with deep convection, occurring near and just after maxima in satellite rainfall data composites around the locations of EO occurrence (not shown). Jakob *et al.* [2005] also showed a relationship between tropical convective activity and mid-level clouds at the near-equatorial Manus Atmospheric Radiation Measurement (ARM) site. Furthermore, deep (convective) EO tops, not just layer cloud tops, show a second peak near -15°C (thin line in Figure 2a), and deep echo profiles (Figure 1b) also indicate a weak second mode near -15°C in box D, not just box E. Of course, a microphysical explanation could still underlie both tower and layer clouds, so this finding is not definitive indication of enhanced detrainment. Meanwhile, convection can detrain mass at levels below its top, so a detrainment

hypothesis for the layer enhancement need not hinge on finding an enhancement of cumulus tops.

[24] The main environmental control on detrainment is thought to be static stability [Bretherton and Smolarkiewicz, 1989]. We sought stability anomalies in composite ECMWF-AUX temperature profiles in association with the two sub-populations of layer-like EOs topping near the 0°C level and the -15°C level. A slight broad stability enhancement (lapse rate decrease) does emerge around the altitude of whichever EO type is used as the composite basis, but the results are subtle and inconclusive (not shown). In any case, a stable-layer association with cloud enhancement would not constitute an explanation, since a layer of cloud creates a stable layer near its top by radiative cooling, and a peak in climatological stable layer occurrence near -15°C would be harder to explain than the cloudiness peak itself. Clear-air radiation and dynamics have no sharp temperature dependences, so some condensed-water effects must ultimately underlie these sharp fine structures tied to temperature.

[25] The most obvious sharp-in-temperature process in the atmosphere is melting of precipitation near 0°C . Might the -15°C echo top peak be an example of the forced gravity wave “melting layer reverberations” in the vertical, as discussed by Mapes and Houze [1995]? They provided a dynamical signal - vertically sharp midlevel wind divergence in Doppler radar data - as the actual observation, so detailed comparison to present results is impossible. Experiments with melting-like sharp forcings could be done in cloud resolving models with high vertical resolution grids, to see if the ensemble effect is to create cloud enhancements 2–3 km above.

[26] As a way forward observationally, phase discrimination of clouds near -15°C might offer more clues. Lidar data from CALIPSO [Winker and Pelon, 2003] could detect

small liquid droplets missed by the CloudSat CPR. Lidar depolarization from CALIPSO can help discriminate particle phase [Cho *et al.*, 2008]. Standard ice water content (IWC) and liquid water content (LWC) CloudSat products are much too crude to advance the case, as they currently assume a simple linear transition from water to ice between 0°C and -20°C [Wood, 2008]. There is clearly room for improvement in our understanding of mixed-phase and ice microphysics, and a robust global signature like that documented here may offer a good target for theory, observation, and models.

[27] **Acknowledgments.** Paquita Zuidema, Robin Hogan, and anonymous reviewers provided invaluable discussions. This work was performed under a subcontract from the Jet Propulsion Laboratory, California Institute of Technology, sponsored by the National Aeronautics and Space Administration.

References

- Bretherton, C. S., and P. K. Smolarkiewicz (1989), Gravity waves, compensating subsidence and detrainment around cumulus clouds, *J. Atmos. Sci.*, *46*, 740–759.
- Cho, H., P. Yang, G. W. Kattawar, S. L. Nasiri, Y. Hu, P. Minnis, C. Trepte, and D. Winker (2008), Depolarization ratio and attenuated backscatter for nine cloud types: Analyses based on collocated CALIPSO lidar and MODIS measurements, *Optics Express*, *16*, 3931–3948.
- Fukuta, N., and T. Takahashi (1999), The growth of atmospheric ice crystals: A summary of findings in vertical supercooled cloud tunnel studies, *J. Atmos. Sci.*, *56*, 1963–1979.
- Hanna, J. W., D. M. Schultz, and A. R. Irving (2008), Cloud-top temperatures for precipitating winter clouds, *J. Appl. Meteorol. Climatol.*, *47*, 351–359.
- Haynes, J. M., and G. L. Stephens (2007), Tropical oceanic cloudiness and the incidence of precipitation: Early results from CloudSat, *Geophys. Res. Lett.*, *34*, L09811, doi:10.1029/2007GL029335.
- Hogan, R. J., P. N. Francis, H. Flentje, A. J. Illingworth, M. Quante, and J. Pelon (2003), Characteristics of mixed-phase clouds I: Lidar, radar and aircraft observations from CLARE'98, *Q. J. R. Meteorol. Soc.*, *129*, 2089–2116.
- Hogan, R. J., M. P. Mittermaier, and A. J. Illingworth (2006), The retrieval of ice water content from radar reflectivity factor and temperature and its use in evaluating a mesoscale model, *J. Appl. Meteorol. Climatol.*, *45*, 301–317.
- Hollars, S., Q. Fu, J. Comstock, and T. Ackerman (2003), Comparison of cloud-top height from ground-based 35 GHz MMCR and GMS-5 satellite observations and ARM TWP Manus site, *Atmos. Res.*, *72*, 169–186.
- Im, E., S. L. Durden, and C. Wu (2005), Cloud profiling radar for the CloudSat mission, *IEEE Trans. Aerosp. Electron. Syst.*, *20*, 15–18.
- Jakob, C., G. Tselioudis, and T. Hume (2005), The radiative, cloud, and thermodynamic properties of the major tropical western Pacific cloud regimes, *J. Clim.*, *18*, 1203–1215.
- Johnson, R. H., T. M. Rickenback, S. A. Rutledge, P. E. Ciesielski, and W. H. Schubert (1999), Trimodal characteristics of tropical convection, *J. Clim.*, *12*, 2397–2418.
- Mapes, B. E., and R. A. Houze (1995), Diabatic divergence profiles in western Pacific mesoscale convective systems, *J. Atmos. Sci.*, *52*, 1807–1828.
- Marchand, R. T., G. Mace, T. Ackerman, and G. L. Stephens (2008), Hydrometeor detection using CloudSat: An Earth orbiting 94 GHz cloud radar, *J. Atmos. Oceanic Technol.*, *25*, 519–533.
- Rogers, R. R., and M. K. Yau (1989), *A Short Course in Cloud Physics*, 3rd ed., 350 pp., Butterworth-Heinemann, Woburn, Mass.
- Ryan, B. F., E. R. Wishart, and D. E. Shaw (1976), The growth rates and densities of ice crystals between -3°C and -21°C , *J. Atmos. Sci.*, *33*, 842–850.
- Sassen, K., and V. I. Khvorostyanov (2007), Microphysical and radiative properties of mixed-phase altocumulus: A model evaluation of glaciation effects, *Atmos. Res.*, *84*, 390–398.
- Sassen, K., Z. Wang, and D. Liu (2008), Global distribution of cirrus clouds from CloudSat/Cloud-Aerosol Lidar and Infrared Pathfinder Satellite Observations (CALIPSO) measurements, *J. Geophys. Res.*, *113*, D00A12, doi:10.1029/2008JD009972.
- Stephens, G. L., et al. (2002), The CloudSat mission and the A-Train, *Bull. Am. Meteorol. Soc.*, *83*, 1771–1790.
- Stephens, G. L., et al. (2008), CloudSat mission: Performance and early science after the first year of operation, *J. Geophys. Res.*, *113*, D00A18, doi:10.1029/2008JD009982.
- Winker, D. M., and J. Pelon (2003), The CALIPSO mission: Spaceborne lidar for observation of aerosols and clouds, *Proc. SPIE Int. Soc. Opt. Eng.*, *4893*, 1–11.
- Wood, N. (2008), Level 2B Radar-Visible Optical Depth Cloud Water Content (2B-CWC-RVOD) process description document, 26 pp., Coop. Inst. for Res. in the Atmos., Fort Collins, Colo.
- Zuidema, P. (1998), The 600–800 mb minimum in tropical cloudiness observed during TOGA COARE, *J. Atmos. Sci.*, *55*, 2220–2228.

B. E. Mapes and E. M. Riley, Department of Meteorology and Physical Oceanography, University of Miami, Miami, FL 33149, USA. (eriley@rsmas.miami.edu)